Neural Computing and Applications
https://doi.org/10.1007/s00521-024-09704-z

ORIGINAL ARTICLE

Vibration analysis and control of aircraft landing systems using proposed neural controllers

Şahin Yıldırım[1] · Aslı Durmuşoğlu[2]

Received: 14 August 2023 / Accepted: 25 March 2024
© The Author(s) 2024

Abstract
Nowadays, landing gears used in aircraft are the basic systems that carry the weight of aircraft systems and provide them to move on the ground. During the landing of aircraft, big and sudden vibrations occur as soon as the wheels come into contact with the runway. This situation negatively affects human safety, comfort and also the life of the landing gear system. Therefore, it is important to keep this vibration at permissible levels. This paper presents an improved vibration control method that controls the amplitudes of vibrations of landing systems. This paper presents proposed vibration control method that controls the angular position variables of the landing gear mechanism to control the vibrations occurring during landing. For different runway conditions and 200 km/h landing speed, the angular joint variables of the landing gear mechanism links are controlled using standard controller and a proposed neural controller structure. The simulation results are shown that the proposed neural controllers have better performance at vibration control of landing systems during landing.

Keywords Neural networks · System analysis · Airplane landing system · Neural controller · Gear mechanism

1 Introduction

The aircraft landing gear is the most important part of the aircraft in terms of safety on land due to its functional mission. The first task of the landing gear is to absorb the horizontal and vertical kinetic energy, ensuring stability and safety on the runway. For this reason, with the advent of modern aircraft, more efficient landing gears have been developed. Due to the increasing weight and landing speeds of aircraft, energy dissipation has become necessary to protect the fuselage from ground loads on the runway.

Shimmy dampers are passive solutions for unwanted roll vibrations in the aircraft landing gear. Although they dampen vibrations substantially, when added to existing landing gear systems, they can bring weight, cost and safety issues. Li et al. [1] have been designed a device to dampen the shimmy vibrations that occur in the main landing gear. They developed a nonlinear mathematical model to represent the landing gear dynamics. As a result of the analysis, it has been seen that the proposed device is more efficient than conventional dampers. Rahmani and Behdinan [2] have been presented a new damper concept. The designed damper is suitable for installation on the existing landing gear and includes damping units. In another study, they have been investigated the effect of torque link Freeplay on the Coulomb frictions that occur in the nose landing gear [3]. Tourajizedeh and Zare [4] have been performed robust and optimal control of shimmy vibrations in the nose landing gear.

Vibration in the aircraft's landing gear causes fatigue tension in its mechanical elements. This causes high wear and damage to the landing gear components. Orlando [5] has been proposed an adaptive controller that damps vibrations under disturbing effects to prevent this security problem. Laporte et al. [6] has designed a landing gear free from the dynamic behaviour of shimmy vibrations. Huynh et al. [7] have been presented a new active controller to

✉ Şahin Yıldırım
sahiny@erciyes.edu.tr

Aslı Durmuşoğlu
aslidurmusoglu@hakkari.edu.tr

[1] Department of Mechatronics Engineering, Engineering Faculty, Erciyes University, 38000 Kayseri, Turkey

[2] Department of Mechanical Engineering, Engineering Faculty, Hakkari University, 30000 Hakkari, Turkey

Published online: 25 April 2024

prevent roll oscillations occurring in the nose landing gear. Simulations have shown that the controller can effectively dampen shimmy vibrations for different scenarios. Wang et al. [8] have been developed a mathematical model to control aircraft vibrations occurring due to disturbances in the runway. According to the results of the simulation, the impact loads and the vertical displacement of the aircraft formed instantly reduced with the use of the active controller. Luong et al. [9] have been used genetic algorithm and artificial neural networks (ANN) controllers for the control of MR damper landing gear. Analysis results have been revealed the effectiveness of the designed controller. Jo et al. [10] have been developed a two degree of freedom model to validate the performance of MR dampers for light aircraft landing gear. Lee et al. [11] have been used a different approach in their study and modelled the behaviour of the MR damper landing gear under irregular impacts during taxiing with Monte Carlo analysis. Viet et al. [12] have been researched sliding mode control for MR damper landing gear.

The stability of the aircraft during taxiing, as well as during landing and take-off, is one of the important issues in the development of aircraft. Sivakumar and Haran [13] have been examined the vibrations occurring in the landing gear of unmanned aerial vehicles in their study. They investigated the optimization of aircraft mass and torsional damping under the influence of shimmy vibrations. Thus, it is aimed to extend the life of the landing gear and prevent potential risks related to oscillations. In another study, they have been analysed random vibrations in the random ground profile of passive and active landing gear [14]. The results obtained in the study showed that the vibration level in the active landing gear was lower than in the conventional landing gear. Yazıcı and Sever [15] have been performed active vibration control for a full aircraft model with 11 degrees of freedom. They designed an observation-based optimal controller with the linear matrix inequities approach to dampen the vibrations originating from the ground during taxiing. Simulation results showed that the proposed controller reduces vibration amplitudes in the aircraft fuselage. Quang-Ngoc et al. [16] have been controlled the aircraft landing gear equipped with MR damper with intelligent control and model predictive control approach. They used these two different control approaches to solve the nonlinear behaviour and delay time problems in the MR tipper semi-active landing gear.

In the literature, it is possible to come across many studies aimed at dampening the vibrations called shimmy that aircrafts are exposed to. In this sense, in addition to the existing suspension systems of the landing gear, ER and MR dampers were integrated to dampen vibrations. In this study, it is aimed to contribute to the literature by controlling the angular position variables of the landing gear mechanism, in addition to the semi-active suspension systems in the passenger aircraft landing gear. Simulations were made for two different landing speeds and different runway pavement surfaces. The equations of the angular joint variables of the six-linked landing gear mechanism were obtained, and transfer functions and state-spaces were created. The landing gear system was modelled in the Simulink environment under the influence of disturbances (aerodynamic and reaction forces). While analysing the landing gear subject to the study, the A320 model aircraft of Airbus company, which is the most popular passenger aircraft in the fleets of airline companies around the world, was taken as reference.

The motivation in this study is that the aircraft is exposed to very big vibrations during landing, and this is an undesirable situation for both aircraft equipment and passengers in terms of comfort and safety. Unlike other studies, the novelty of this article is that the angular displacement of the landing gear mechanism is controlled by the proposed controller. In this study, a neural network control system for aircraft landing gear's vibration control is proposed. The paper firstly explains the dynamic of the landing gear mechanism. Then, the proposed neural controller and PID controller are defined. The results of proposed neural control system and PID control system are presented and debated. In conclusion, the efficiency of proposed control method is determined.

2 Dynamic of the landing gear mechanism

To explain the dynamics of a landing gear mechanism, four degrees of freedom (DOF) mathematical model is used and is presented in Fig. 1. The model, containing the link lengths (L_2, L_3, L_4, L_5 and L_6), angular joint variables (θ_2, θ_3, θ_4, θ_5 and θ_6), link mass (m_2, m_3, m_4, m_5 and m_6) and external forces (F_f, N) of the landing gear mechanism.

As shown in Fig. 1, Link 2 and Link 3 represent the side-stay strut. Link 4 and Link 5 denote the unlock mechanism, and Link 6 is the main strut. The main strut contains the support shaft and shock absorber. The strut, which is described as the leg of the landing gear, supports the shaft together with the shock absorber. Structural parameters of the Airbus A320 aircraft main landing gear are given in Table 1.

The dynamics of the landing gear mechanism is derived using Lagrangian equations.

$$\mathcal{L} = K_E - P_E. \tag{1}$$

The Euler–Lagrangian equations can be solved by taking partial derivatives of the kinetic energy and potential energy properties of the system. Thus, the equation of motion of the system is obtained.

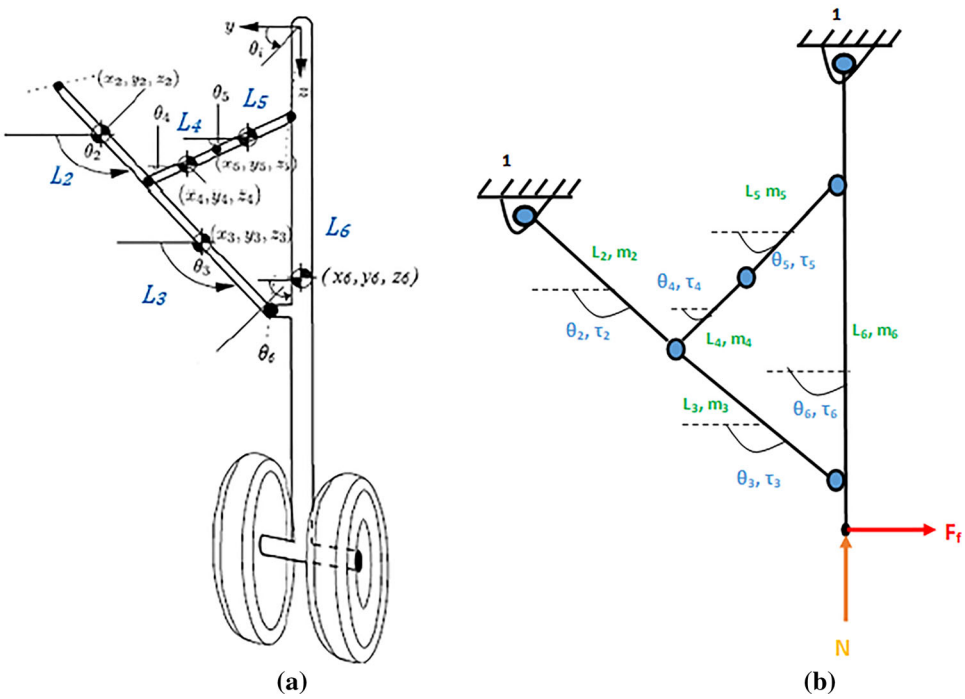

Fig. 1 **a** Landing gear mechanism axis and angular joint variables and **b** physical model of the landing gear system

Table 1 Landing gear mechanism structural parameters [17]

Parameter	Value	Unit
L_2	2200	mm
L_3	1310	mm
L_4	980	mm
L_5	960	mm
L_6	2540	mm
m_2	108	kg
m_3	122	kg
m_4	32	kg
m_5	30	kg
m_6	270	kg
θ_2	2.3	rad
θ_3	2.1	rad
θ_4	0.7	rad
θ_5	0.6	rad
θ_6	1.6	rad
N	70,000	kgf
V	200	m/sn
μ_{asphalt}	0.5	
μ_{concrete}	0.3	

$$\frac{\mathrm{d}}{\mathrm{d}(t)} = \left(\frac{\partial \mathcal{L}}{\partial \dot{\theta}_n}\right) - \frac{\partial \mathcal{L}}{\partial \dot{\theta}_n} = \tau_n. \tag{2}$$

where θ_n is the angular joint variable of joints, and τ_n is the torque applied to the links. The positions of the links are calculated as a function of the angular joint variables in the Y–Z coordinate plane using the forward kinematic equations.

$$y_2 = L_2 \cdot \cos\theta_2, \tag{3}$$

$$z_2 = -L_2 \cdot \sin\theta_2, \tag{4}$$

$$y_3 = L_2 \cdot \cos\theta_2 + L_3 \cdot \cos(\theta_2 + \theta_3), \tag{5}$$

$$z_3 = -L_2 \cdot \sin\theta_2 - L_3 \cdot \sin(\theta_2 + \theta_3), \tag{6}$$

$$y_4 = L_2 \cdot \cos\theta_2 + L_4 \cdot \cos(\theta_4 + \theta_2), \tag{7}$$

$$z_4 = -L_2 \cdot \sin\theta_2 - L_4 \cdot \sin(\theta_4 + \theta_2), \tag{8}$$

$$y_5 = L_6 \cdot \cos\theta_6 + L_5 \cdot \cos(\theta_5 + \theta_6), \tag{9}$$

$$z_5 = -L_6 \cdot \sin\theta_6 - L_5 \cdot \sin(\theta_5 + \theta_6), \tag{10}$$

$$y_6 = L_6 \cdot \cos\theta_6, \tag{11}$$

$$z_6 = -L_6 \cdot \sin\theta_6. \tag{12}$$

Kinetic and potential energy equations of L_2 link;

$$K_{E2} = \frac{1}{2} m_2 {L_2}^2 \dot{\theta}_2^2, \tag{13}$$

$$P_{E2} = m_2 g L_2 \sin\theta_2. \tag{14}$$

Kinetic and potential energy equations of L_3 link;

$$K_{E3} = \frac{1}{2} m_3 L_2^2 \dot{\theta}_2^2 + \frac{1}{2} m_3 L_3^2 (\dot{\theta}_2 + \dot{\theta}_3)^2 + m_3 L_2 L_3 \left(\dot{\theta}_2^2 + \dot{\theta}_2 \dot{\theta}_3\right) \cos\theta_3, \tag{15}$$

$$P_{E3} = -m_3 g L_2 \sin\theta_2 - m_3 g L_3 \sin(\theta_2 + \theta_3). \tag{16}$$

Kinetic and potential energy equations of L_4 link;

$$K_{E4} = \frac{1}{2}m_4L_2^2\dot{\theta}_2^2 + \frac{1}{2}m_4L_4^2(\dot{\theta}_2 + \dot{\theta}_4)^2 + m_4L_2L_4\left(\dot{\theta}_2^2 + \dot{\theta}_2\dot{\theta}_4\right)\cos\theta_4, \quad (17)$$

$$P_{E4} = -m_4gL_2\sin\theta_2 - m_4gL_4\sin(\theta_2 + \theta_4). \quad (18)$$

Kinetic and potential energy equations of L_5 link;

$$K_{E5} = \frac{1}{2}m_5L_6^2\dot{\theta}_6^2 + \frac{1}{2}m_5L_5^2(\dot{\theta}_5 + \dot{\theta}_6)^2 + m_5L_2L_5\left(\dot{\theta}_6^2 + \dot{\theta}_5\dot{\theta}_6\right)\cos\theta_5, \quad (19)$$

$$P_{E5} = -m_5gL_6\sin\theta_5 - m_5gL_5\sin(\theta_6 + \theta_5). \quad (20)$$

Kinetic and potential energy equations of L_6 link;

$$K_{E6} = \frac{1}{2}m_6{L_6}^2\dot{\theta}_6^2, \quad (21)$$

$$P_{E6} = m_6gL_6\sin\theta_6. \quad (22)$$

These energy equations are created to the Lagrangian equations, and the following nonlinear equations of the landing gear mechanism are obtained.

$$\mathcal{L}_{23} = K_{E2} + K_{E3} - P_{E2} - P_{E3}, \quad (23)$$

$$\mathcal{L}_{23} = \frac{1}{2}m_2{L_2}^2\dot{\theta}_2^2 + \frac{1}{2}m_3L_2^2\dot{\theta}_2^2 + \frac{1}{2}m_3L_3^2\left(\dot{\theta}_2 + \dot{\theta}_3\right)^2 + m_3L_2L_3\left(\dot{\theta}_2^2 + \dot{\theta}_2\dot{\theta}_3\right)\cos\theta_3 - m_3gL_2\sin\theta_2 - m_3gL_3\sin(\theta_2 + \theta_3) - m_2gL_2\sin\theta_2 + m_3gL_2\sin\theta_2 + m_3gL_3\sin(\theta_2 + \theta_3). \quad (24)$$

$$\mathcal{L}_{24} = K_{E2} + K_{E4} - P_{E2} - P_{E4}, \quad (25)$$

$$\mathcal{L}_{24} = \frac{1}{2}m_2{L_2}^2\dot{\theta}_2^2 + \frac{1}{2}m_4L_2^2\dot{\theta}_2^2 + \frac{1}{2}m_4L_4^2\left(\dot{\theta}_2 + \dot{\theta}_4\right)^2 + m_4L_2L_4\left(\dot{\theta}_2^2 + \dot{\theta}_2\dot{\theta}_4\right)\cos\theta_4 - m_2gL_2\sin\theta_2 + m_3gL_2\sin\theta_2 + m_3gL_3\sin(\theta_2 + \theta_3). \quad (26)$$

$$\mathcal{L}_{65} = K_{E6} + K_{E5} - P_{E6} - P_{E5}, \quad (27)$$

$$\mathcal{L}_{65} = \frac{1}{2}m_6{L_6}^2\dot{\theta}_6^2 + \frac{1}{2}m_5L_6^2\dot{\theta}_6^2 + \frac{1}{2}m_5L_5^2(\dot{\theta}_5 + \dot{\theta}_6)^2 + m_5L_2L_5\left(\dot{\theta}_6^2 + \dot{\theta}_5\dot{\theta}_6\right)\cos\theta_5 - m_6gL_6\sin\theta_6 + m_5gL_6\sin\theta_5 + m_5gL_5\sin(\theta_6 + \theta_5). \quad (28)$$

Using the Lagrangian equation, the torque forces of the five links are obtained as follows.

$$\tau_2 = \left((m_2 + m_3)L_2^2 + m_3L_3^2 + 2m_3L_2L_3\cos\theta_3\right)\ddot{\theta}_2 + \left(m_3L_3^2 + m_3L_2L_3\cos\theta_3\right)\ddot{\theta}_3 - m_3L_2L_3\left(2\dot{\theta}_2\dot{\theta}_3 + \dot{\theta}_3^2\right)\sin\theta_3 + (m_2 - m_3)gL_2\cos\theta_2 - m_3gL_3\cos(\theta_2 + \theta_3), \quad (29)$$

$$\tau_3 = m_3L_3^2\ddot{\theta}_3 + \left(m_3L_3^2 + m_3L_2L_3\cos\theta_3\right)\ddot{\theta}_2 + m_3L_2L_3\ddot{\theta}_2^2\sin\theta_3 - m_3gL_3\cos(\theta_2 + \theta_3), \quad (30)$$

$$\tau_4 = m_4L_4^2\ddot{\theta}_4 + \left(m_4L_4^2 + m_4L_2L_4\cos\theta_4\right)\ddot{\theta}_2 + m_4L_2L_4\ddot{\theta}_2^2\sin\theta_4 - m_4gL_4\cos(\theta_2 + \theta_4), \quad (31)$$

$$\tau_5 = m_5L_5^2\ddot{\theta}_5 + \left(m_5L_5^2 + m_5L_6L_5\cos\theta_5\right)\ddot{\theta}_6 + m_5L_6L_5\ddot{\theta}_6^2\sin\theta_5 - m_5gL_5\cos(\theta_6 + \theta_5), \quad (32)$$

$$\tau_6 = \left((m_6 + m_5)L_6^2 + m_5L_5^2 + 2m_5L_6L_5\cos\theta_5\right)\ddot{\theta}_6 + \left(m_5L_5^2 + m_5L_6L_5\cos\theta_5\right)\ddot{\theta}_5 - m_5L_6L_5\left(2\dot{\theta}_6\dot{\theta}_5 + \dot{\theta}_5^2\right)\sin\theta_5 + (m_6 - m_5)gL_6\cos\theta_6 - m_5gL_5\cos(\theta_6 + \theta_5). \quad (33)$$

The second-order differential equations describing the movement of the landing gear mechanism are given as follows.

$$\ddot{\theta}_2 = \frac{1}{\left((m_2 + m_3)L_2^2 + m_3L_3^2 + 2m_3L_2L_3\cos\theta_3\right)}[\tau_1 - \left(m_3L_3^2 + m_3L_2L_3\cos\theta_3\right)\ddot{\theta}_3 + m_3L_2L_3\left(2\dot{\theta}_2\dot{\theta}_3 + \dot{\theta}_3^2\right)\sin\theta_3 - (m_2 - m_3)gL_2\cos\theta_2 + m_3gL_3\cos(\theta_2 + \theta_3), \quad (34)$$

$$\ddot{\theta}_3 = \frac{1}{m_3L_3^2}[\tau_3 - \left(m_3L_3^2 + m_3L_2L_3\cos\theta_3\right)\ddot{\theta}_2 - m_3L_2L_3\ddot{\theta}_2^2\sin\theta_3 + m_3gL_3\cos(\theta_2 + \theta_3), \quad (35)$$

$$\ddot{\theta}_4 = \frac{1}{m_4L_4^2}[\tau_4 - \left(m_4L_4^2 + m_4L_2L_4\cos\theta_4\right)\ddot{\theta}_2 - m_4L_2L_4\ddot{\theta}_2^2\sin\theta_4 + m_4gL_4\cos(\theta_2 + \theta_4), \quad (36)$$

$$\ddot{\theta}_5 = \frac{1}{m_5L_5^2}[\tau_5 - \left(m_5L_5^2 + m_5L_6L_5\cos\theta_5\right)\ddot{\theta}_6 - m_5L_6L_5\ddot{\theta}_6^2\sin\theta_5 + m_5gL_5\cos(\theta_6 + \theta_5), \quad (37)$$

$$\ddot{\theta}_6 = \frac{1}{\left((m_6 + m_5)L_6^2 + m_5L_5^2 + 2m_5L_6L_5\cos\theta_5\right)}[\tau_6 - \left(m_5L_5^2 + m_5L_6L_5\cos\theta_5\right)\ddot{\theta}_5 + m_5L_6L_5\left(2\dot{\theta}_6\dot{\theta}_5 + \dot{\theta}_5^2\right)\sin\theta_5 - (m_6 - m_5)gL_6\cos\theta_6 + m_5gL_5\cos(\theta_6 + \theta_5). \quad (38)$$

External forces acting on the landing gear mechanism can be defined as friction force and ground reaction force. The torque that occurs in the joints due to the effect of external forces can be calculated using the inverse of the Jacobian matrix.

$$F_f = \mu_k \cdot N, \quad (39)$$

$$\tau_T = \tau + J^T \cdot F_{ex}, \tag{40}$$

$$J^T \cdot F_{ex} = \begin{bmatrix} \frac{\partial y_3}{\partial \theta_2} & \frac{\partial z_3}{\partial \theta_2} \\ \frac{\partial y_3}{\partial \theta_3} & \frac{\partial z_3}{\partial \theta_3} \end{bmatrix} \cdot \begin{bmatrix} F_f \\ N \end{bmatrix}. \tag{41}$$

where F_f is the friction force, N is the ground reaction force, F_{ex} is the external forces, μ_k is the friction coefficient of the ground, τ_T is the total torque and J^T is the transpose of the Jacobian matrix.

3 Control systems

In this study, angular joint variables of the landing gear mechanism are controlled, and different control organs are used to approximate the variables to the reference value. The transfer functions and state-spaces of the angular joint variables, which are detailed in Sect. 2, are presented below. Angular joint variable transfer function and state-space of L_2 link;

$$\frac{\theta_2(s)}{\tau_2(s)} = \frac{-148s^2 + 1275s + 5574}{250s^4 + 288s^3 + 354.5s^2 + 11.5s + 8.054}, \tag{42}$$

$$\boldsymbol{A} = \begin{bmatrix} -1.1528 & -1.4188 & -0.0460 & -0.0324 \\ 1 & 0 & 0 & 0 \\ 0 & 1 & 0 & 0 \\ 0 & 0 & 1 & 0 \end{bmatrix},$$

$$\boldsymbol{B} = \begin{bmatrix} 1 \\ 0 \\ 0 \\ 0 \end{bmatrix},$$

$$\boldsymbol{C} = [0 \quad -0.5919 \quad 50.9968 \quad 22.2962], \boldsymbol{D} = 0. \tag{43}$$

Angular joint variable transfer function and state-space of L_3 link;

$$\frac{\theta_3(s)}{\tau_3(s)} = \frac{-137s^2 + 1135s + 5244}{230s^4 + 271s^3 + 334.5s^2 + 10.5s + 7.154}, \tag{44}$$

$$\boldsymbol{A} = \begin{bmatrix} -1.1326 & -1.3842 & -0.0360 & -0.0221 \\ 1 & 0 & 0 & 0 \\ 0 & 1 & 0 & 0 \\ 0 & 0 & 1 & 0 \end{bmatrix},$$

$$\boldsymbol{B} = \begin{bmatrix} 1 \\ 0 \\ 0 \\ 0 \end{bmatrix},$$

$$\boldsymbol{C} = [0 \quad -0.4819 \quad 47.9458 \quad 18.2232], \boldsymbol{D} = 0. \tag{45}$$

Angular joint variable transfer function and state-space of L_4 link;

$$\frac{\theta_4(s)}{\tau_4(s)} = \frac{-9.8s^3 + 268s^2 + 13.28s - 8.587}{210s^4 + 204s^3 + 214.5s^2 + 9.5s + 7.054}, \tag{46}$$

$$\boldsymbol{A} = \begin{bmatrix} -1.0728 & -1.3210 & -0.0660 & -0.0424 \\ 1 & 0 & 0 & 0 \\ 0 & 1 & 0 & 0 \\ 0 & 0 & 1 & 0 \end{bmatrix},$$

$$\boldsymbol{B} = \begin{bmatrix} 1 \\ 0 \\ 0 \\ 0 \end{bmatrix},$$

$$\boldsymbol{C} = [0 \quad -0.4219 \quad 38.2468 \quad 17.2322], D = 0. \tag{47}$$

Angular joint variable transfer function and state-space of L_5 link;

$$\frac{\theta_5(s)}{\tau_5(s)} = \frac{-9.8s^3 + 268s^2 + 13.28s - 7.5427}{210s^4 + 204s^3 + 214.5s^2 + 9.5s + 6.154}, \tag{48}$$

$$\boldsymbol{A} = \begin{bmatrix} -1.0728 & -1.3210 & -0.0660 & -0.0317 \\ 1 & 0 & 0 & 0 \\ 0 & 1 & 0 & 0 \\ 0 & 0 & 1 & 0 \end{bmatrix},$$

$$\boldsymbol{B} = \begin{bmatrix} 1 \\ 0 \\ 0 \\ 0 \end{bmatrix},$$

$$\boldsymbol{C} = [0 \quad -0.4219 \quad 38.2468 \quad 17.1722], \quad D = 0. \tag{49}$$

Angular joint variable transfer function and state-space of L_6 link;

$$\frac{\theta_6(s)}{\tau_6(s)} = \frac{-273.5s^2 + 181s + 9.337}{254s^4 + 298.2s^3 + 354.5s^2 + 11.5s + 8.092}, \tag{50}$$

$$\boldsymbol{A} = \begin{bmatrix} -1.1728 & -1.6188 & -0.0260 & -0.0224 \\ 1 & 0 & 0 & 0 \\ 0 & 1 & 0 & 0 \\ 0 & 0 & 1 & 0 \end{bmatrix},$$

$$\boldsymbol{B} = \begin{bmatrix} 1 \\ 0 \\ 0 \\ 0 \end{bmatrix},$$

$$\boldsymbol{C} = [0 \quad -0.6319 \quad 52.9968 \quad 24.9162], D = 0. \tag{51}$$

The closed-loop control block diagram for the control of the angular joint variables of the landing gear is given in

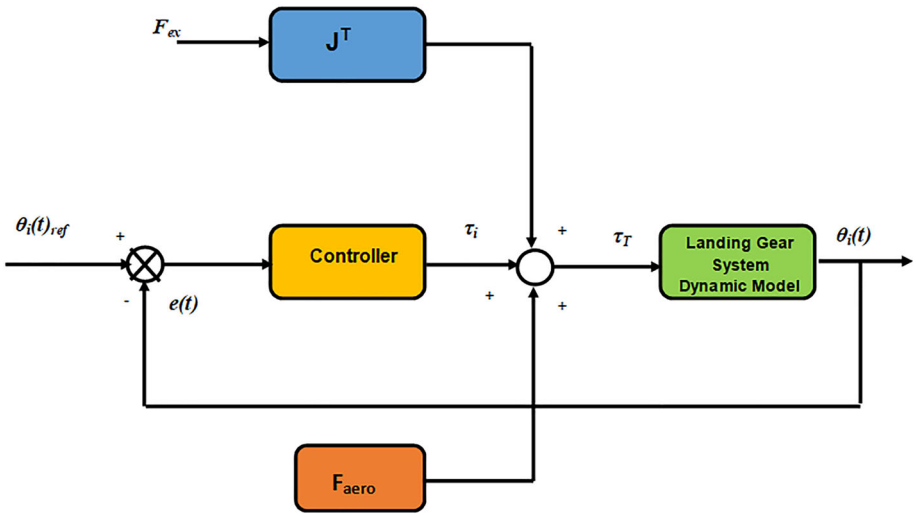

Fig. 2 Closed-loop control block diagram

Table 2 Friction coefficients of different runway pavement surfaces [19]

Aspalth pavement (μ_{aspalth})	Concrete pavement (μ_{concrete})
0.5	0.3

Fig. 2. The input value of the block diagram is the reference value of the angular joint variable. Ground reaction force and aerodynamic forces during landing are defined as disturbance magnitudes. With the input of the controller, the appropriate torque force is produced and given as an input to the dynamic model. The dynamic model calculates the available joint angles and uses them as feedback to the controller. The damping has been neglected while performing the analyses, and the maximum force that the aircraft can be exposed to at the moment of landing on the runway has been taken into account. In this study, analysis is performed for asphalt (μ_{asphalt}) and concrete (μ_{concrete}) and pavement surfaces under the control of the angular joint variables of the landing gear mechanism. The friction coefficients for these runway pavements are given in Table 2 [19].

Here θ_i(t)ref is the reference value of ith link angular joint variable, θ_i(t) is the output of the control system, τ_i is the torque of ith link, τ_T is the total torque, F_{ex} is the external forces acting on the landing gear system and F_{aero} is the aerodynamic force.

3.1 PID controller

PID controller comprises proportional P(e(t)), integral I(e(t)) and derivative D(e(t)) sections. It is a control effect that combines the superiorities of three main control effects under a single unit. The control signal u(t) produced by the controller is time-dependent and is given by:

$$u(t) = K_p e(t) + K_i \int_0^t e(t) + K_d \frac{de(t)}{dt}. \tag{52}$$

The $e(t)$ function, which is defined as the error function, is the difference between desired response and the actual response, and it changes depending on time. K_p is denoted proportional gain, K_i is the integral gain and K_d is the derivative gain. Also, Zeigler–Nichols methods are used to settle the optimum PID gain parameters. PID gain parameters are presented in Table 3.

3.2 Neural network controller

A neural network controller typically includes two stages: system definition and control designing. The feed-forward

Table 3 PID gain parameters

Angular joint variables	K_p		K_i		K_d	
	μ_{aspalth}	μ_{concrete}	μ_{aspalth}	μ_{concrete}	μ_{aspalth}	μ_{concrete}
θ_2	1.63	1.57	0.7	0.65	0.074	0.06
θ_3	1.6	1.49	0.65	0.6	0.07	0.053
θ_4	1.4	1.31	0.44	0.42	0.042	0.04
θ_5	1.91	1.9	0.51	0.39	0.035	0.033
θ_6	1.98	1.98	0.85	0.83	0.093	0.09

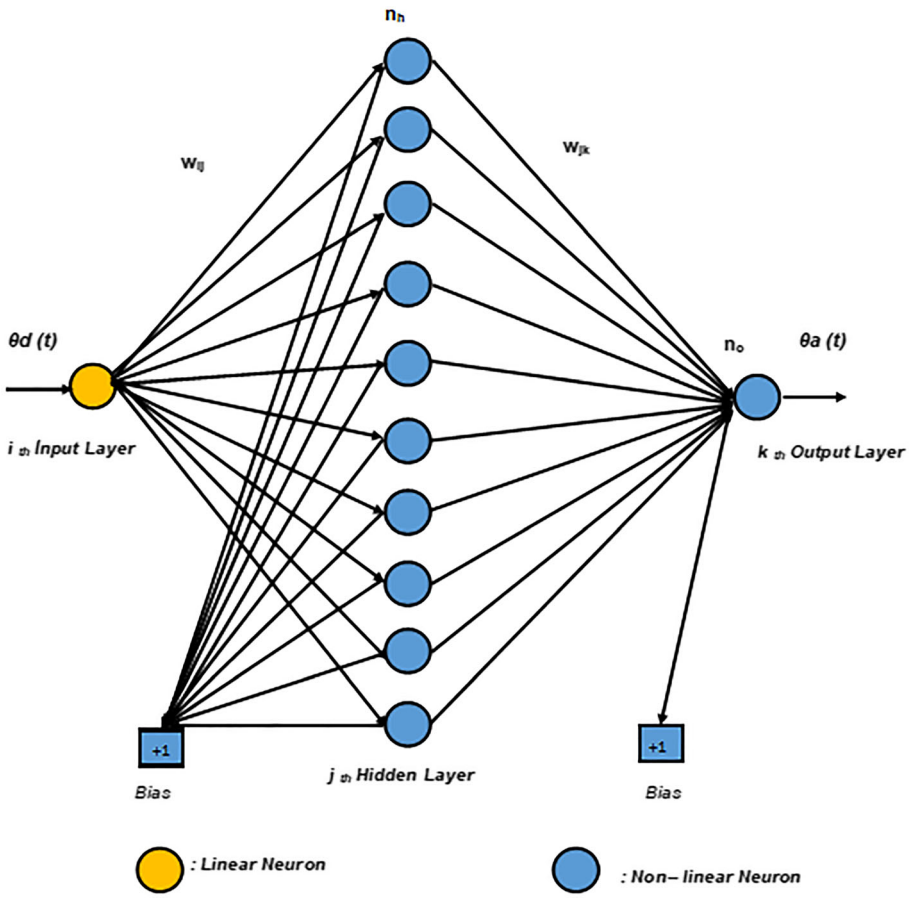

Fig. 3 Schematic representation of feed-forward neural network structure

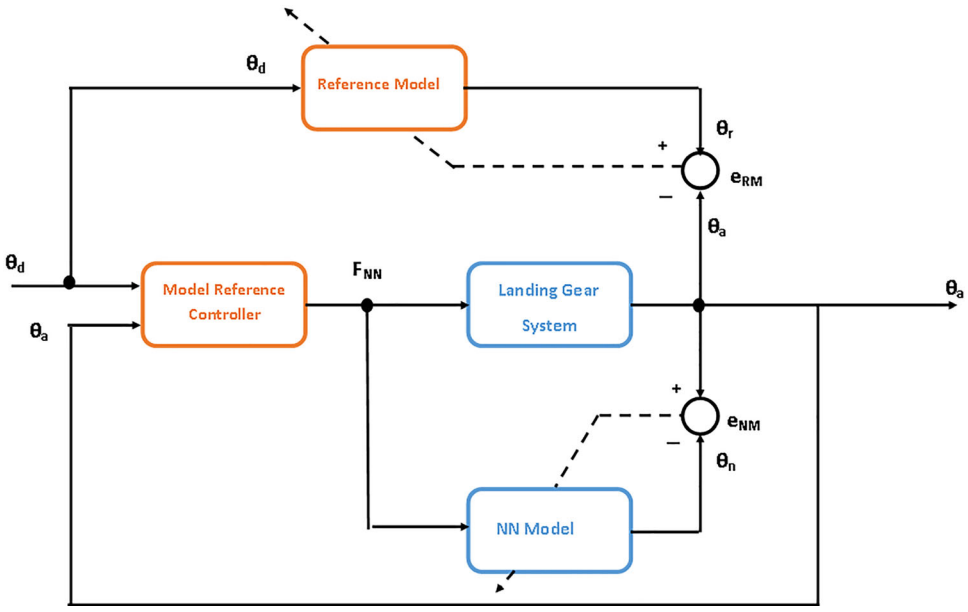

Fig. 4 Block diagram of model reference controller

neural network structure is used to control the angular joint variables of the landing gear mechanism. The schematic view of the developed neural network model is given in Fig. 3.

The output of the hidden layer;

$$Z_j(t) = f\left[\sum_{i=1}^{10} [\theta_i(t)w_{1j}(t) + \theta_g(t)w_{2j}] + 1\right]. \quad (53)$$

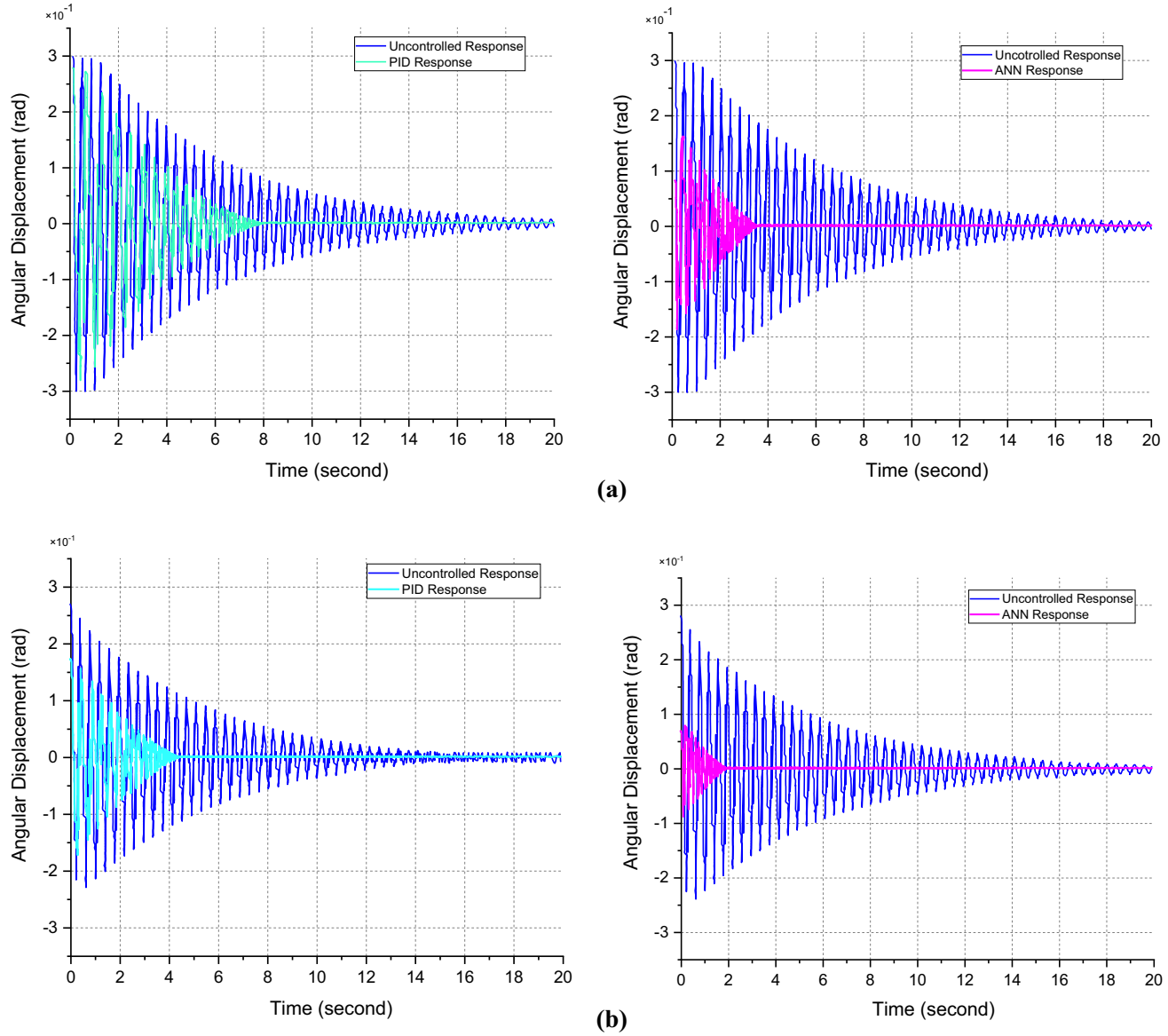

Fig. 5 PID and ANN response of θ_2 angular joint variables, **a** $\mu_{\text{asphalt}} = 0.5$ and **b** $\mu_{\text{concrete}} = 0.3$

The output of this layer is passed through the nonlinear activation function. The output of the hidden layer;

$$f(x) = \frac{2}{(1 + e^{-2x})} - 1, \tag{54}$$

$$Z_j(t) = \frac{2}{\left(1 + e^{-2\left[\sum_{i=1}^{10} [\theta_i(t) w_{1j}(t) + \theta_g(t) w_{2j}] + 1\right]}\right)} - 1. \tag{55}$$

The output signal of the output layer can be written as;

$$\theta_g(t) = \sum_{j=1}^{10} Z_j(t) w_{j1}(t) + 1. \tag{56}$$

The output signal of neural network model;

$$\theta_g(t) = \sum_{j=1}^{10} \left[\left[\frac{2}{\left(1 + e^{-2\left[\sum_{i=1}^{10} [\theta_i(t) w_{1j}(t) + \theta_g(t) w_{2j}] + 1\right]}\right)} - 1 \right] w_{j1}(t) + 1 \right]. \tag{57}$$

Here w_{1j} is the weight matrix between the input layer and the hidden layer, and w_{2j} is the weight matrix between the hidden layer and the output layer [18]. In the neural network model, there is one linear neuron in the input layer, 10 nonlinear neurons in the hidden layer and one nonlinear neuron in the output layer. The number of iterations is determined as 1,000,000, and η (learning rate) is 0.1.

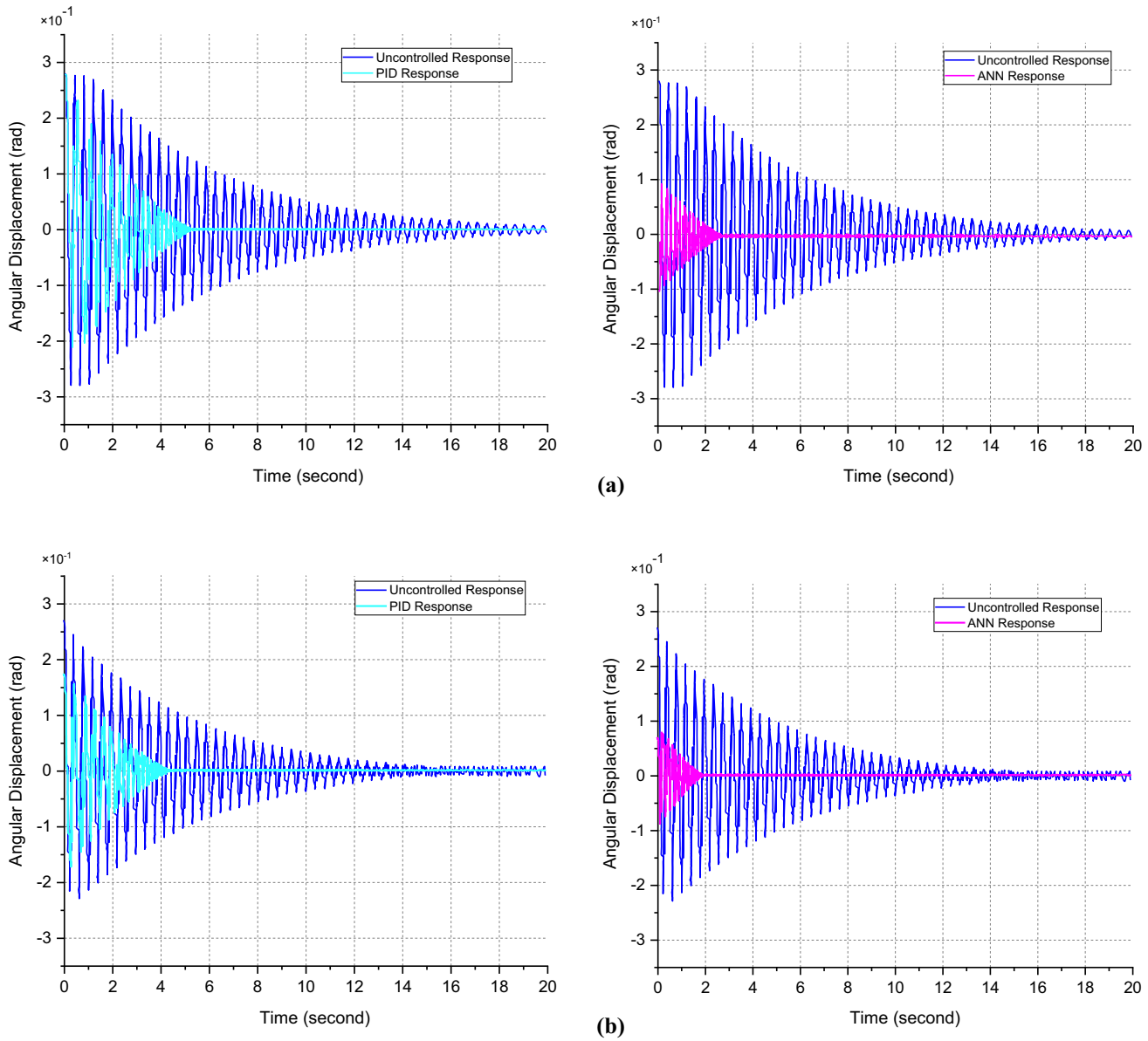

Fig. 6 PID and ANN response of θ_3 angular joint variables, **a** $\mu_{\text{asphalt}} = 0.5$ and **b** $\mu_{\text{concrete}} = 0.3$

3.3 Levenberg–Marquardt (LM) algorithm

The Levenberg–Marquardt algorithm is used to randomly change the weights of the network. The Levenberg–Marquardt algorithm, like the Quasi-Newton methods, uses the approximate value of the Hessian matrix [18]. The approximate value of the Hessian matrix for the Levenberg–Marquardt algorithm can be found as follows:

$$H(t) = J^{\mathrm{T}}(t)J(t) + \mu I_H. \tag{58}$$

μ is the Marquardt parameter, and H is the unit matrix. J is called the Jacobian matrix and consists of the first derivatives of the network errors according to the weights.

$$J(t) = \frac{\partial e(t)}{\partial w(t-1)}. \tag{59}$$

$e(t)$ is the vector of network errors. The Jacobian matrix is preferred as it is easier to compute than the Hessian matrix. The gradient of the network is calculated as follows,

$$g(t) = J^{T}(t)e(t). \tag{60}$$

3.4 Model reference neural network control

The model reference neural network control organ is used as a mathematical model for comparison with the actual control system. In this neural network plant model, an error

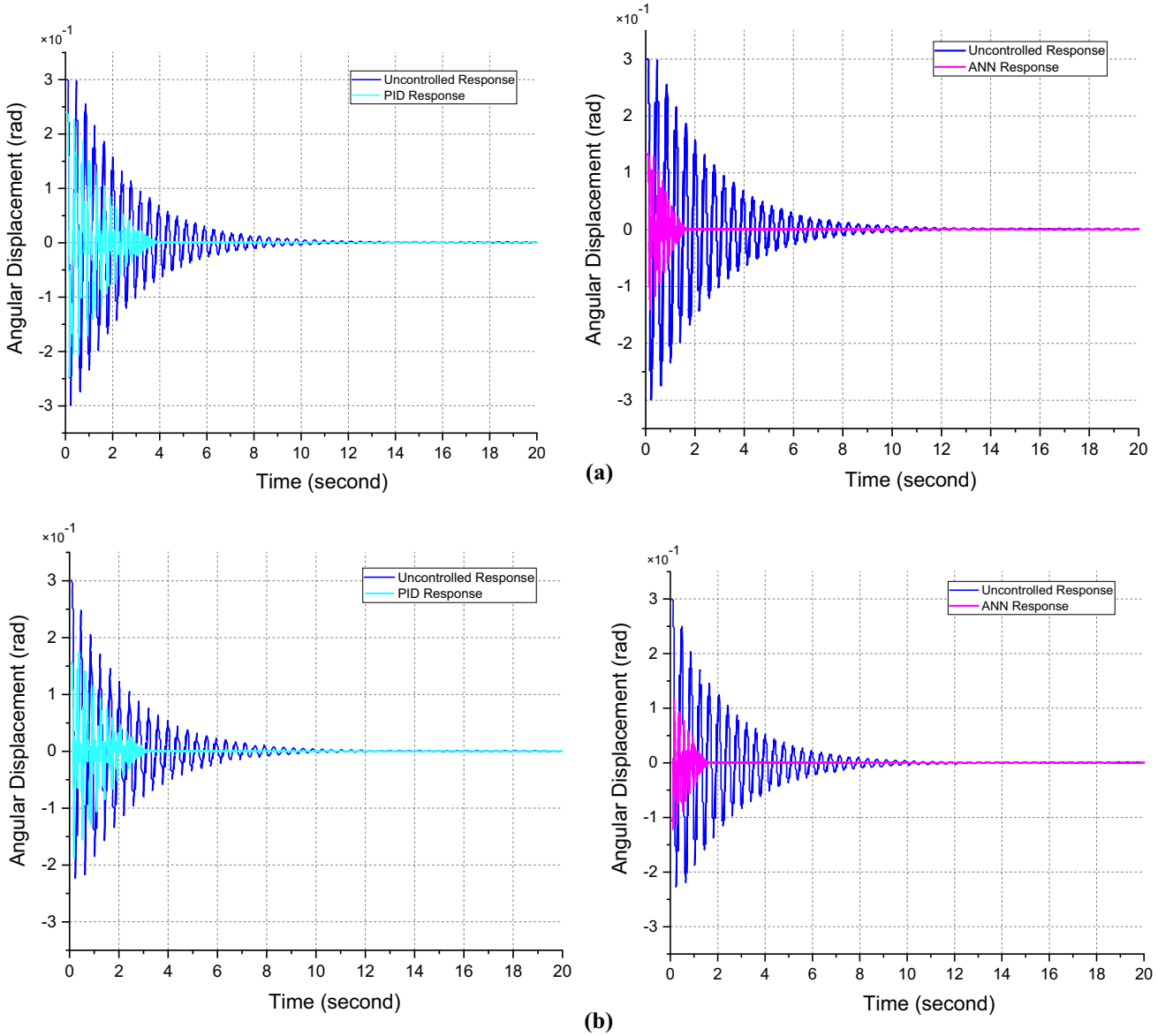

Fig. 7 PID and ANN response of θ_4 angular joint variables, **a** $\mu_{\text{asphalt}} = 0.5$ and **b** $\mu_{\text{concrete}} = 0.3$

is generated based on the difference between the actual and model outputs. The control law of the model reference neural network controller is as follows;

$$\tau_{NN}(t) = \sum_{j=1}^{10} \left[\left[\frac{2}{\left(1 + e^{-2\left[\sum_{i=1}^{10} [\theta_i(t) w_{1j}(t) + \theta_g(t) w_{2j}] + 1\right]}\right)} - 1 \right] w_{j1}(t) + 1 \right]. \tag{61}$$

The Levenberg–Marquardt algorithm is used to adjust the weights in the feed-forward neural network. The block diagram of the model reference control system is schematically given in Fig. 4.

where e_{RM} is the reference model error, e_{NM} is the error of the landing gear system model, $\theta_i(t)$ is the desired position input signal of the landing gear system, $\theta_g(t)$ is the actual position input signal of the landing gear system, $\theta_r(t)$ is the output signal of the reference model and $\theta_n(t)$ is the output signal of the neural network model. Here, a third-order system is chosen as the reference model transfer function of the system. The Laplace domain of this reference model can be given as follows;

$$G(s) = \frac{0.2s + 2}{s^3 + 71.5s^2 + 113.05s + 455.5}. \tag{62}$$

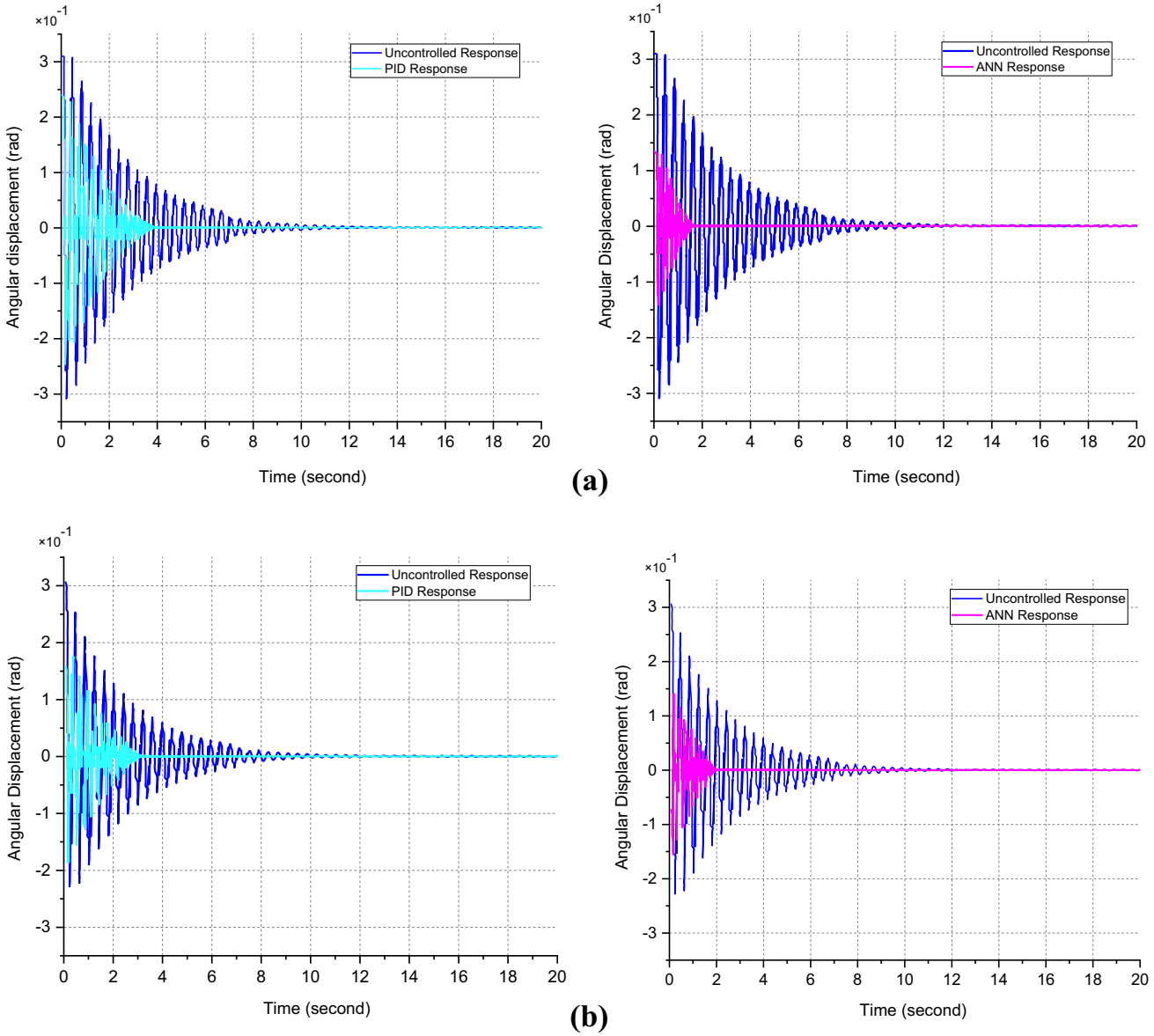

Fig. 8 PID and ANN response of θ_5 angular joint variables, **a** $\mu_{\text{asphalt}} = 0.5$ and **b** $\mu_{\text{concrete}} = 0.3$

4 Simulation results

4.1 PID and ANN responses

The simulations are performed for two different runway coefficients and 200 km/h landing speed. At the first moment, the landing gear puts wheels on the runway, the suspension system acts rigid and the landing gear system is subjected to the greatest force. While performing the analyses, the damping effect in the wheel and suspension is neglected, and simulations are made for the maximum value of the reaction force. It is aimed to approximate the angular joint variables of the landing gear mechanism to the reference values by using the PID controller and the neural network controller. The simulation results for the control of angular joint variables with PID controller and neural network controller are given in Figs. 5, 6, 7, 8 and 9. In Fig. 5, the PID and ANN control responses of the θ_2 angular joint variable of the lateral strut are presented. As shown in Fig. 5a and b, ANN shows better performance than PID in the analysis for different runway friction coefficients. In asphalt runway pavement, the system shows a stable state after 4 s and the response speed decreased to 2 s on the concrete pavement with a neural network controller.

Figure 6a and b gives the result of the PID and ANN control system for θ_3 angular joint variables. When the system responses under the PID control effect are

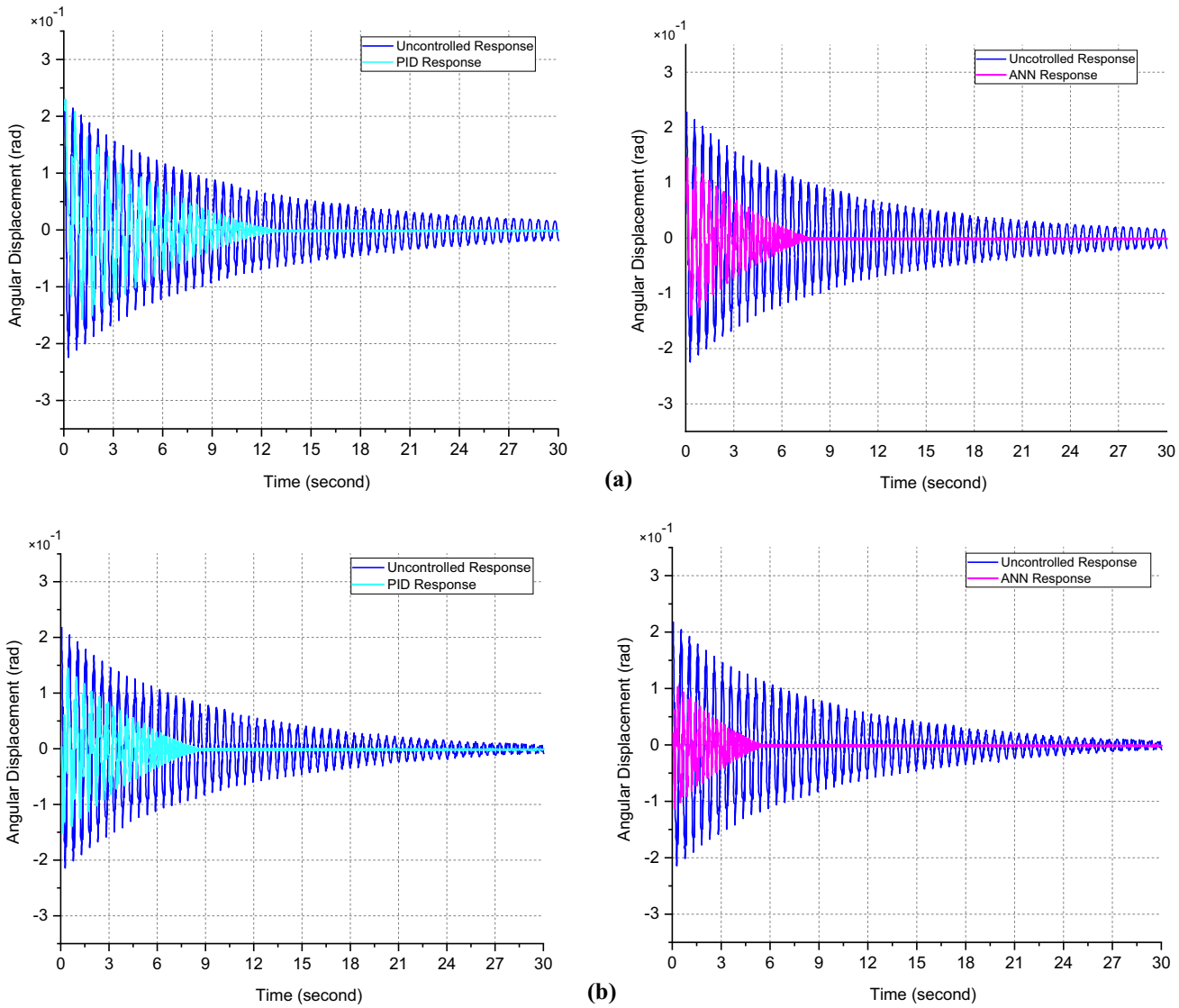

Fig. 9 PID and ANN response of θ_6 angular joint variables, **a** $\mu_{\text{asphalt}} = 0.5$ and **b** $\mu_{\text{concrete}} = 0.3$

examined, it is seen that the damping effect is obtained in the range of 2–4 s, and the system becomes stable. Besides, with the ANN controller, a stable behaviour was exhibited in approximately 2 s for all runway conditions.

The result of PID and ANN control for θ_4 angular joint variables is given in Fig. 7a and b. As described in Fig. 7a and b, uncontrolled system outputs are unstable, and the neural network controller has a good performance at stability on both runway pavements. It is seen clearly, there are differences between PID and ANN controller. The results of the PID controller are weak to control compared to the neural network controller.

Response of PID and ANN controller for θ_5 angular joint variables is given in Fig. 8a and b. As shown in Fig. 8a, the response of the system reached the desired value in the asphalt runway pavement in the 4th second with the PID controller. On the other hand, the damping effect with neural network control is observed in 2 s. Similarly, on concrete pavement, the neural network controller is suitable for controlling the angular displacement.

Lastly, Fig. 9a and b is demonstrated the response of the angular displacement of the landing gear main strut. When the graphs are examined, it is seen that uncontrolled system output magnitudes are raising. As shown in Fig. 9a, there is a stable behaviour in the 8th second with a neural network controller. Otherwise, the PID controller exhibits stable behaviour at 12th seconds. As seen in the relevant figure for concrete pavement, it is observed that the response times of both control organs are reduced. Reaction forces and moments act directly on the landing gear strut. Due to these reasons, both controllers have a late response time.

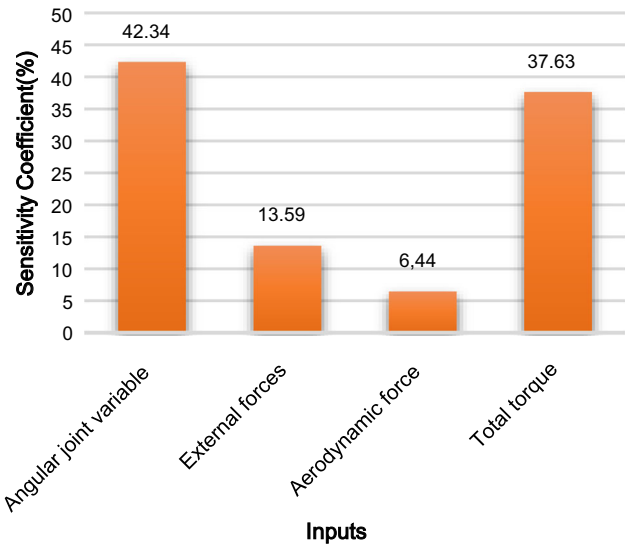

Fig. 10 The sensitivity coefficients of each input parameter

The simulation results show that the highest vibration occurred in the main strut of the landing gear system. This is because external forces act directly on the main strut. The least angular displacement values are observed in the unlock mechanism.

4.2 Sensitivity analysis

In the proposed ANN control model, a sensitivity analysis based on the algorithm called the Garson algorithm [20] was performed to analyse the effect of inputs on the output. Thus, the contribution of each input parameter in vibration control of the aircraft landing system was analysed. In this algorithm, the sensitivity coefficient can be calculated as follows:

$$Q_{ik}\frac{\sum_{j=1}^{L}\left(\left|w_{ij}v_{jk}\right|/\sum_{r=1}^{N}\left|w_{rj}v_{jk}\right|\right)}{\sum_{i=1}^{N}\sum_{j=1}^{L}\left(\left|w_{ij}v_{jk}\right|/\sum_{r=1}^{N}\left|w_{rj}v_{jk}\right|\right)}. \tag{63}$$

where Q_{ik} represents the sensitivity coefficient of the input i to the output k, w_{ij}, and v_{jk} represents the weights from input variable i to hidden neuron j and from hidden neuron j to the output k, respectively. L represents the number of neurons in the hidden layer, and N indicates input variables.

Sensitivity coefficients of all input parameters are presented in Fig. 10. As shown in Fig. 10, the most critical parameters affecting the control of the aircraft landing system are angular position variables and total torque values. The sensitivity coefficients of these values are 42.34% and 37.63%, respectively. External forces acting on the aircraft during landing are the next most important factor with a sensitivity coefficient of 13.59%. Aerodynamic force, on the other hand, has the lowest effect on landing gear vibration control with a sensitivity coefficient of 6.44%. The input parameters selected for an optimal model should reflect all factors affecting vibration control performance. However, choosing too many parameters may increase the complexity of the ANN model and negatively affect its accuracy and response time. With sensitivity analysis, the effect of each input parameter on the output parameter was revealed. Thus, the aerodynamic force parameter with the lowest effect on the output parameter was determined. The sensitivity analysis results provided the reference for developing a high accuracy and extensively feasible control model in controlling the aircraft landing system.

5 Conclusions and discussion

In this paper, neural networks and standard control systems are applied for aircraft landing gear vibration control. The landing gear mechanism is regarded as four degrees of freedom system. PID and ANN are compared for asphalt and concrete runway pavement. The proposed ANN control system is comprised of a feed-forward neural network predictive controller and model reference neural network controller. Standard control methods cannot adapt to disruptive factors because they have constant parameters and are insufficient in controlling complex systems. Therefore, it is more appropriate to use an adaptive ANN structure for the control and analysis of complex and nonlinear systems, and optimum control can be achieved. From the simulation results, it is seen that using ANN control system with a feedback controller and model reference neural network controller, high vibration control performance can be achieved for all runway conditions. In controlling the angular joint variables of the landing gear mechanism, the ANN control system is achieved superior performance than the standard PID control system because of its adaptive structure.

Funding Open access funding provided by the Scientific and Technological Research Council of Türkiye (TÜBİTAK).

Data availability The datasets generated during and analysed during the current study are available from the corresponding author on reasonable request.

Declarations

Conflict of interest The authors declare that they have no conflict of interest concerning the publication of this manuscript.

Open Access This article is licensed under a Creative Commons Attribution 4.0 International License, which permits use, sharing, adaptation, distribution and reproduction in any medium or format, as

long as you give appropriate credit to the original author(s) and the source, provide a link to the Creative Commons licence, and indicate if changes were made. The images or other third party material in this article are included in the article's Creative Commons licence, unless indicated otherwise in a credit line to the material. If material is not included in the article's Creative Commons licence and your intended use is not permitted by statutory regulation or exceeds the permitted use, you will need to obtain permission directly from the copyright holder. To view a copy of this licence, visit http://creativecommons.org/licenses/by/4.0/.

References

1. Li Y, Howcroft C, Neild SA, Jiang JZ (2017) Using continuation analysis to identify shimmy-suppression devices for an aircraft main landing gear. J Sound Vib 408:234–251. https://doi.org/10.1016/j.jsv.2017.07.028
2. Rahmani M, Behdinan K (2019) Parametric study of a novel nose landing gear shimmy damper concept. J Sound Vib 457:299–313. https://doi.org/10.1016/j.jsv.2019.06.008
3. Rahmani M, Behdinan K (2020) Interaction of torque link Freeplay and Coulomb friction nonlinearities in nose landing gear shimmy scenarios. Int J Non-Linear Mech 119:103338. https://doi.org/10.1016/j.ijnonlinmec.2019.103338
4. Tourajizadeh H, Zare S (2016) Robust and optimal control of shimmy vibration in aircraft nose landing gear. Aerosp Sci Technol 50:1–14. https://doi.org/10.1016/j.ast.2015.12.019
5. Orlando C (2020) Nose landing gear simple adaptive shimmy suppression system. J Guid Control Dyn 43(7):1–15. https://doi.org/10.2514/1.G004832
6. Laporte DJ, Lopes V, Bueno DD (2020) An approach to reduce vibration and avoid shimmy on landing gears based on an adapted eigenstructure assignment theory. Meccanica 55(1):7–17. https://doi.org/10.1007/s11012-019-01101-4
7. Huynh TH, Pouly G, Lauffenburger JP, Basset M (2008) Active shimmy damping using direct adaptive fuzzy control. IFAC Proceedings Volumes 41(2):15052–15057. https://doi.org/10.3182/20080706-5-KR-1001.02547
8. Wang H, Xing JT, Price WG, Li W (2008) An investigation of an active landing gear system to reduce aircraft vibrations caused by landing impacts and runway excitations. J Sound Vib 317(1–2):50–66. https://doi.org/10.1016/j.jsv.2008.03.016
9. Luong QV, Jang DS, Hwang JH (2020) Intelligent control based on a neural network for aircraft landing gear with a magnetorheological damper in different landing scenarios. Appl Sci 10(17):5962. https://doi.org/10.3390/app10175962
10. Jo BH, Jang DS, Hwang JH, Choi YH (2021) Experimental validation for the performance of MR damper aircraft landing gear. Aerospace 8(9):272. https://doi.org/10.3390/aerospace8090272
11. Lee HS, Jang DS, Hwang JH (2020) Monte carlo simulation of MR damper landing gear taxiing mode under nonstationary random excitation. Journal of Aerospace System Engineering 14(4):10–17. https://doi.org/10.20910/JASE.2020.14.4.10
12. Viet LQ, Lee HS, Jang DS, Hwang JH (2020) Sliding mode control for an ıntelligent landing gear equipped with magnetorheological damper. Journal of Aerospace System Engineering 14(2): 20–27. https://doi.org/10.20910/JASE.2020.14.2.20
13. Sivakumar S, Haran AP (2015) Aircraft random vibration analysis using active landing gears. Journal Of Low Frequency Noıse, Vıbratıon And Actıve Control 34(3):307–322. https://doi.org/10.1260/0263-0923.34.3.307
14. Sivakumar S, Ganapathy Subramanian LR, Giridharan V (2024) Shimmy vibration analysis of unmanned aircraft coupled with landing gears. J Mech Sci Technol 38(1):1–11. https://doi.org/10.1007/s12206-023-12
15. Yazıcı H, Sever M (2016) Observer based optimal vibration control of a full aircraft system having active landing gears and biodynamic pilot model. Shock Vib 2016:1–20. https://doi.org/10.1155/2016/2150493
16. Quang-Ngoc L, Hyeong-Mo P, Yeongjin K, Huy-Hoang P, Jai-Hyuk H, Quoc-Viet L (2023) An ıntelligent control and a model predictive control for a single landing gear equipped with a magnetorheological damper. Aerospace 10(11):951. https://doi.org/10.3390/aerospace10110951
17. Sivakumar S, Haran AP (2015) Mathematical model and vibration analysis of aircraft with active landing gears. J Vib Control 21(2):229–245. https://doi.org/10.1177/10775463134869
18. Eski İ, Yıldırım Ş (2009) Vibration control of vehicle active suspension system using a new robust neural network control system. Simul Model Pract Theory 17:778–793. https://doi.org/10.1016/j.simpat.2009.01.004
19. Ledbetter RH (1975) Pavement response to aircraft dynamic loads. Army Engıneer Waterways Experıment Statıon Vıcksburg Mıss 2.
20. Parrales A, Colorado D, Díaz-Gómez JA, Huicochea A, Álvarez A, Hernández JA (2018) New void fraction equations for two-phase flow in helical heat exchangers using artificial neural networks. Appl Therm Eng 130:149–160. https://doi.org/10.1016/j.applthermaleng.2017.10.139

Publisher's Note Springer Nature remains neutral with regard to jurisdictional claims in published maps and institutional affiliations.